Luminescence emission from forward- and reverse-biased multicrystalline silicon solar cells

K. Bothe, K. Ramspeck, D. Hinken, C. Schinke, J. Schmidt, S. Herlufsen, R. Brendel, J. Bauer, J.-M. Wagner, N. Zakharov, and O. Breitenstein

Luminescence emission from forward- and reverse-biased multicrystalline silicon solar cells

K. Bothe,[1,a)] K. Ramspeck,[1,b)] D. Hinken,[1] C. Schinke,[1] J. Schmidt,[1] S. Herlufsen,[1] R. Brendel,[1] J. Bauer,[2] J.-M. Wagner,[2] N. Zakharov,[2] and O. Breitenstein[2]

[1]*Institut für Solarenergieforschung Hameln (ISFH), Am Ohrberg 1, D-31860 Emmerthal, Germany*
[2]*Max Planck Institute of Microstructure Physics, Weinberg 2, D-06120 Halle, Germany*

We study the emission of light from industrial multicrystalline silicon solar cells under forward and reverse biases. Camera-based luminescence imaging techniques and dark lock-in thermography are used to gain information about the spatial distribution and the energy dissipation at pre-breakdown sites frequently found in multicrystalline silicon solar cells. The pre-breakdown occurs at specific sites and is associated with an increase in temperature and the emission of visible light under reverse bias. Moreover, additional light emission is found in some regions in the subband-gap range between 1400 and 1700 nm under forward bias. Investigations of multicrystalline silicon solar cells with different interstitial oxygen concentrations and with an electron microscopic analysis suggest that the local light emission in these areas is directly related to clusters of oxygen. © *2009 American Institute of Physics.* [doi:10.1063/1.3256199]

I. INTRODUCTION

Since solar cells are large area devices, spatially resolved information on their electrical properties is indispensable in research and development. Imaging techniques for a spatially resolved analysis of silicon wafers and solar cells have become one of the most attractive characterization tools in solar cell research and production over the past decade. In this work, electroluminescence (EL) and dark lock-in thermography (DLIT) imaging of forward- and reverse-biased multicrystalline silicon (mc-Si) solar cells are used to gain a deeper understanding of the physical origin of local pre-breakdown sites. Assuming an ideal abrupt junction and a base doping concentration between 5×10^{15} and 1×10^{16} cm^{-3}, one would expect a breakdown voltage in the range of 90–60 V.[1] In case one silicon solar cell in a string of a solar module is shadowed or partly broken, this cell is reverse biased by the other cells in that string to about 10–20 V in reverse.[2] Therefore, the breakdown voltage of a solar cell should be considerably higher. Especially in mc-Si solar cells, breakdown is often observed at considerably lower voltages and preferentially occurs at localized spots. Large current flows through these pre-breakdown sites result in the formation of so-called microplasmas, which are accompanied by the emission of visible light in the wavelength range between 500 and 1000 nm.[3–5] At the same time, the current flow also results in local heating.[6] In photovoltaic modules, the temperature of those *hot spots* might become high enough to cause a damage in the module encapsulation. Thus, the breakdown voltage at which the current exceeds a certain level is an important parameter for the classification of solar cells. Using lock-in thermography, hot spots have been found to occur preferentially in dislocation-rich areas.[7] Interestingly, luminescence emission in the wavelength range between 1500 and 1700 nm, resulting from radiative recombination via defect states in the band gap, is also primarily found in areas of high dislocation density.[8] Whether the origins of the subband-gap luminescence and the local pre-breakdown are the same has not been investigated in detail so far. Therefore, using luminescence imaging and DLIT, this work focuses on the correlation between areas of high dislocation density characterized by a low band-to-band luminescence under forward bias, a local luminescence emission under reverse bias, and the occurrence of hot spots.

II. LIGHT EMISSION FROM REVERSE- AND FORWARD-BIASED *P-N* JUNCTIONS

Pre-breakdown effects and the emission of light from reverse-biased silicon *p-n* junctions have been widely investigated in the mid 1950s and 1960s aiming at understanding charge multiplication effects in semiconductors. Under forward bias, in addition to band-to-band luminescence, subband-gap luminescence at around 0.8 eV was observed in the vicinity of dislocations even at room temperature. Due to its relevance for optoelectronic applications, this phenomenon was revisited in more detail in the 1990s. Only within the past few years, the analysis of light emission from reverse- and forward-biased mc-Si solar cells has attracted the attention of several research groups[8–11] after camera-based luminescence imaging has been introduced as a versatile tool in photovoltaics in 2005.[12]

A. Light emission from reverse-biased *p-n* junctions

Light emission from reverse-biased *p-n* junctions is closely related to electrical breakdown.[13,14] The breakdown of *p-n* junctions in silicon is usually characterized by microplasma currents,[15,16] which are often accompanied by the emission of light.[3–5] As shown in Fig. 1, two breakdown mechanisms are distinguished: *avalanche breakdown*

---

a)Electronic mail: k.bothe@isfh.de.
b)Present address: SCHOTT Solar AG, Carl-Zeiss-Str. 4, D-63755 Alzenau, Germany.
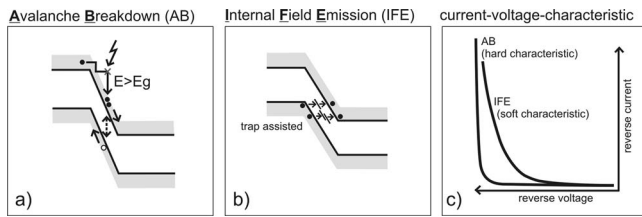
FIG. 1. Diagrams of AB and IFE. (a) AB, $\times$ denotes the position where charge multiplication sets in. (b) IFE, defect states within the band gap reduce the voltage necessary to cross the junction. (c) Resulting current-voltage characteristic of AB and IFE processes.

(AB)[17,18] and *internal field emission* (IFE).[19]

The causes of AB are high electric fields accelerating electrons. The interaction of accelerated electrons with the lattice vibrations of the crystal results in a frictional force opposing the acceleration. Usually, the electrons undergo collisions, which do not allow them to build up sufficient energy to cause ionization. However, if the field strength is high enough, free electrons may gain enough energy within a mean free path to knock a valence band electron out of its bound state and raise it to the conduction band. In case the first electron remains in the conduction band and the process continues, the number of free electrons increases exponentially. Thus, AB is a current multiplication process that can result in the flow of very large currents, limited only by the external circuitry. Therefore, the current-voltage characteristic shows a sudden strong increase, which we will refer to as a *hard characteristic*. In the case of AB, the temperature coefficient (TC)[20] of the breakdown current, describing the change in the absolute value of the current with temperature at constant voltage, is negative if no impurity scattering is involved.[14]

In contrast, IFE occurs in case the electronic bands of a reverse-biased *p-n* junction are tilted, allowing electrons to "long-jump" the forbidden gap by quantum mechanical tunneling. The band gap of a semiconductor decreases with increasing temperature, and thus, less energy is required for the charge carriers to cross the band gap. Moreover, with increasing temperature, the phonon density and consequently the transition probability increase, resulting in a lower breakdown voltage. The IFE is thus characterized by a positive TC of the breakdown current, indicating a larger current flow at higher temperatures. Electronic states within the forbidden gap may considerably increase the probability for electrons to tunnel through the junction, resulting in an IFE at much lower voltages and in a *soft* reverse current-voltage characteristic.

Aiming at a better understanding of the origin of this soft breakdown characteristics and the occurrence of characteristic light emission pattern under reverse bias, the role of crystallographic imperfections and impurities was carefully investigated. The first evidence that the light emission from reverse-biased *p-n* junctions is related to crystal imperfections, especially dislocations, was given by Chynoweth and Pearson.[21] They observed that the emission pattern of reverse-biased diffused *p-n* junctions correlates with the etch-pit patterns displaying dislocations.

A soft breakdown characteristic was found to appear after a specific heat treatment carried out on Czochralski-grown silicon at around 1200 °C followed by a slow cooling.[22] From the current scientific point of view, one might expect that this heat treatment supported the formation of oxygen precipitates having energy states within the band gap. More specifically, the role of oxygen was addressed by Kikuchi and Tachikawa,[23] indicating that the emission of visible light is essentially affected by impurity atoms, in particular by oxygen. Four different breakdown types classified on light emission, multiplication, and microplasma current pulses are distinguished,[24] some of which give rise to light emission while others do not. Preferentially, precipitation of impurities occurs at dislocations and other crystal imperfections.[25] Investigating the impact of metal impurities and precipitates on the reverse current-voltage characteristic of *p-n* junctions, Goetzberger and Shockley[4] identified localized current paths through junctions that were treated in a manner expected to produce metal precipitates. The result of the precipitation treatment was a "softening" of the reverse characteristic due to excess currents below AB.

After Goetzberger and Stephens[26] suggested that the light emitting spots might originate from oxygen precipitated clusters located in the vicinity of dislocations, Shockley[27] gave clear evidence that microplasma and local light emission phenomena under reverse bias are related to structural defects and, in particular, to oxygen precipitates near dense arrays of dislocations.

More recent studies of Akil *et al.*[28,29] address the physical mechanism of junction breakdown, showing that a combined theory of interband processes and Bremsstrahlung is necessary to describe the avalanche emission spectra of reversed bias silicon *p-n* junctions over its whole energy range.

B. Light emission from forward-biased *p-n* junctions

In mc-Si, very high concentrations of dislocations ($>10^8$ cm^{-2}) are typically measured, resulting in an increased local carrier recombination and thus in a strongly reduced carrier lifetime. The impact of dislocations on photoluminescence spectra was first addressed by Drozdov *et al.*,[30] who found that at liquid helium temperature (4 K) dislocations in silicon give rise to four photoluminescence lines labeled D1 (0.812 eV), D2 (0.875 eV), D3 (0.934 eV), and D4 (1.000 eV). Carrier recombination at dislocations occurs primarily due to the presence of metallic impurities.[31–33] First direct evidence for this was given by McHugo *et al.*[34] comparing light beam induced current mappings with synchrotron-based x-ray fluorescence. However, not only metal impurities but also oxygen seems to play a major role. Especially, the broad subband-gap luminescence at around 0.8 eV detectable at room temperature in edge-defined film-fed grown silicon[35] as well as in block-cast mc-Si (Ref. 36) is most likely to be related to thermal donors or oxygen clusters bound to dislocations or trapped in the strain field of dislocations. In a more detailed study, Ostapenko *et al.*[37] reported a very good qualitative correlation of a reduced car-

rier lifetime, strong defect photoluminescence at around 0.8 eV, decreased band-to-band photoluminescence, and enhanced dislocation density.

An increase in the defect band luminescence in the vicinity of dislocations was conclusively explained by the preferential precipitation of oxygen along dislocations.[38] Moreover, it was undoubtedly shown that the origin of the D1/D2 lines found at low temperatures and the defect band at around 0.8 eV detectable at room temperature are different.[38] Oxygen-related room temperature luminescence at around 1600 nm was also reported to appear after prolonged annealing at 450–470 °C of Czochralski-grown silicon[39–41] and after high-temperature processes at around 1200 °C followed by a slow cooling.[42] While the first temperature treatment is known to result in the formation of thermal donors, the latter one typically results in larger oxygen precipitates.

Recently, the structure of the defects responsible for the defect PL band at around 0.8 eV in block-cast mc-Si was investigated by a photoluminescence mapping tomography technique,[43] both at room temperature and at 4 K. It was found that the defects have planelike structures extending in the growth direction. The defects appear as intragrain defects, and it was assumed that they are metal-contaminated dislocation clusters originating from small-angle grain boundaries.

III. EXPERIMENTAL RESULTS

A. Measurement details and setup

The experimental setup consists of a blackened box that is equipped with either of two cameras. While for the luminescence imaging a 640×512 pixel focal plane array InGaAs camera is used, the DLIT measurements are performed using an infrared camera sensitive in the wavelength range from 3.9 to 5 μm. For both measurements, the solar cells are connected to a bipolar power source using a four-point contacting scheme with 25 probes on each bus bar. During the measurements, a thermostat stabilizes the temperature of the solar cell at 25 °C. The DLIT measurements are performed at a lock-in frequency of 20 Hz corresponding to a thermal diffusion length of 1.2 mm in silicon. All EL images are corrected for stray light and dark noise by subtracting a dark image recorded at equal exposure time but with no voltage applied to the cell under test. Detailed descriptions of the physical principles underlying the camera-based DLIT and EL techniques can be found elsewhere.[44–48] Transmission electron microscopy (TEM) images were taken with a Philips CM 20 TWIN TEM, which is equipped with an energy dispersive X-ray (EDX) analysis system by Noran Instruments. The samples under test are 125×125 mm^2 alkaline-textured industrial mc-Si solar cells.

B. Experimental results and discussion

Figure 2 shows luminescence emission images of a block-cast mc-Si solar cell under forward and reverse biases. In image (a) of Fig. 2, the luminescence emission due to band-to-band recombination at 0.6 V forward bias is shown. This EL image shows areas of a strongly reduced EL signal along fine dendritic lines [see, e.g., areas marked by red el-
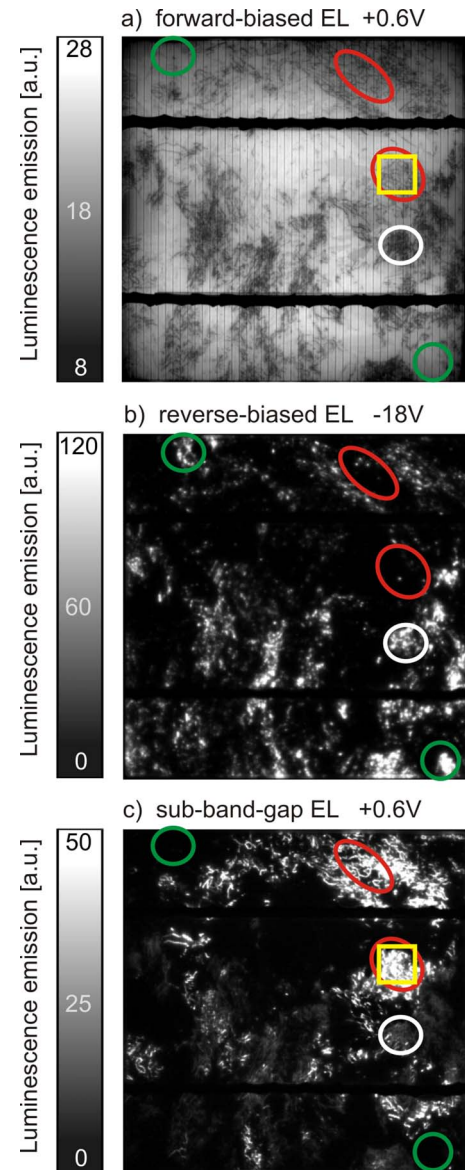

FIG. 2. (Color online) EL images measured at different bias conditions and sample temperatures. (a) EL image at 0.6 V forward bias, (b) luminescence emission image at −16 V reverse bias, and (c) integral (1450–1700 nm) subband-gap luminescence at 0.6 V forward bias.

lipses in Fig. 2(a)] as well as areas with an even higher density of recombination active sites appearing as dark clusters [see, e.g., areas marked by white circle in Fig. 2(a)]. The dendritic lines are typical of mc-Si and originate from intragrain defects such as stacking faults and dislocations. These crystallographic defects are often decorated by impurities or impurity clusters and give rise to an increased nonradiative recombination activity and thus to a decreased EL signal. In those regions appearing as dark clusters, the density of recombination active sites is considerably enhanced such that dendritic lines can hardly be recognized, and it remains unclear whether only the density of dendritic lines is so much higher in these areas or if additional recombination sites are responsible for the low EL signal.

Figure 2(b) shows the light emission image at −16 V reverse bias. As described above, the light emission in the reverse-EL mode is related to local AB or IFE accompanied

by the emission of light. However, more complex mechanisms such as impact ionization of deep states[49,50] and trap-assisted tunneling might also be responsible for the light emission. In regions appearing as dark clusters in the EL image under forward bias [compare, e.g., areas marked white in Figs. 2(a) and 2(b)], we also detect breakdown-related light emission under reverse bias. Figure 2(c) shows the subband-gap luminescence image for the wavelength range between 1450 and 1700 nm at 0.6 V forward bias. Comparing images (a)–(c) of Fig. 2 and especially those areas marked red, it becomes obvious that subband-gap luminescence predominantly occurs in regions characterized by dendritic lines in the EL image and that breakdown-related emission under reverse bias is *not* observed in these regions. These results confirm previous results by Kasemann *et al.*[8] obtained for similar samples using the same characterization techniques.

In conclusion, areas exist where subband-gap luminescence is found independent of the occurrence of breakdown-related luminescence even though a broad distribution of energy states is a preferential situation for trap-assisted tunneling under reverse bias. Thus, on the microscopic scale, the origins of subband-gap luminescence under forward bias and breakdown-related luminescence emission under reverse bias must be different.

As shown in Fig. 3, a spectral analysis of the subband-gap luminescence reveals a broad peak with a maximum at around 1550 nm, indicating a rather broad distribution of energy states with a maximum located at around 0.8 eV away from the conduction or valence band. Similar spectra have previously been published by Tajima,[39] attributing their occurrence to oxygen clusters formed during annealing of Czochralski-grown silicon at around 470 °C, and Koshka *et al.*,[35] investigating multicrystalline edge-defined film-fed grown silicon by photoluminescence linking the 0.8 eV defect band to grain boundaries with accumulated impurities, such as oxygen.

To confirm the existence of oxygen clusters at subband-gap luminescence sites, a TEM sample is prepared out of the area of the solar cell where only subband-gap luminescence was detected. This area is marked by an orange rectangle in Fig. 2. The TEM sample was directly prepared at a cluster of the dendritic lines, as shown in Fig. 2(a). In the investigated area (roughly 100×100 μm^2), four precipitates were found. Figure 4 shows exemplarily a TEM image of one of these precipitates and the corresponding EDX analysis spectra. The spectrum shows a peak at 0.525 keV, which is the oxygen $K\alpha_1$ peak. The EDX analysis at a reference point some hundred nanometers away from the precipitate shows no such oxygen peak. The EDX spectra of the other three precipitates show the same oxygen peak. At both positions, no further EDX peaks are detected for energies up to 40 keV, indicating that metal impurities do not contribute to the subband-gap luminescence.

For wafers with interstitial oxygen concentrations well above 2×10^{17} cm^{-3} as found in the bottom regions of mc-Si blocks, Möller *et al.*[51] reported that oxygen precipitation not only occurs at dislocations but also homogenously distributed in the bulk. Thus, solar cells made out of oxygen-rich
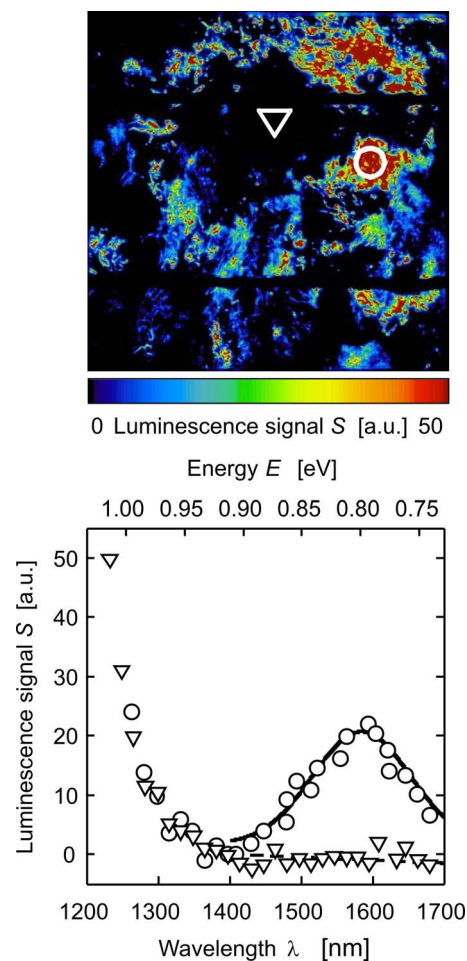

FIG. 3. (Color online) Top: image of the integral luminescence emission in the wavelength range between 1450 and 1700 nm of a mc-Si solar cell (same cell as in Fig. 2) detected at 0.6 V forward bias using an InGaAs camera. Bottom: luminescence spectrum of a representative area showing a high subband-gap luminescence in comparison with an area showing no subband-gap luminescence.

mc-Si wafers should show a homogeneous subband-gap luminescence emission superimposed by a stronger emission at dislocations sites. Investigating block-cast mc-Si solar cells from different block positions and oxygen concentrations, we are able to confirm this assumption experimentally. Figure 5 shows the subband-gap luminescence from three solar cells with oxygen concentration varying between 9×10^{17} and 2×10^{17} cm^{-3} taken from different positions out of the same block. While solar cell (a) from the bottom region of block 1 shows a homogenous subband-gap emission superimposed by some brighter spots, cell (b) from the middle region shows the typical bright local emission. In order to exclude the fact that the position of the cell in the block is important, Fig. 5(c) shows the subband-gap luminescence of a cell taken from the bottom region of a different block but having an interstitial oxygen concentration of only 2×10^{17} cm^{-3}. It should be noted that solar cells from the very bottom region of a mc-Si block show a significantly reduced EL contrast compared to solar cells from the middle or top regions, independent of the interstitial oxygen concentration. Areas with characteristic dendritic lines or dark clusters resulting from twin boundaries accompanied by dislocations and
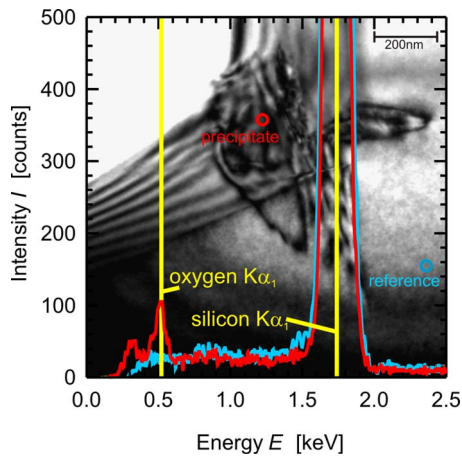
FIG. 4. (Color online) TEM image and EDX spectra from the center of the area marked by orange squares in Fig. 2. This area is characterized by recombination at dendritic lines, which also show strong subband-gap luminescence but no light emission under reverse bias. The EDX spectrum taken of a precipitate located at the crossing point of two dislocation lines shows a clear oxygen $K\alpha_1$ peak (red curve), while no oxygen is found at a reference point (blue curve) some hundred nanometers away. Both regions show the characteristic silicon $K\alpha_1$ peak.

stacking faults[52] are not frequently found in those cells. Since oxygen precipitation predominantly occurs at dislocation clusters, local subband-gap luminescence is more often found in solar cells coming from the middle or top regions of mc-Si blocks.

The light emission under reverse bias may follow from a perturbation of the electronic band structure, which can in general be caused by both metal impurities and oxygen-related defects. While a preference for SiO_x particles situated in the space charge region of the *p-n* junction has recently been published by Wagner and Weber,[53] the incorporation of metal impurities cannot be excluded from the current observations.

The high current flow at local breakdown sites is associated with a local temperature increase. Thus, pre-breakdown sites under reverse bias can be well characterized by dark lock-in thermography (reverse-DLIT).[54] However, the high spatial resolution of the luminescence images showing breakdown sites with diameters of some 10 μm is masked in the DLIT measurements by the heat distribution around the individual spots. Figure 6 shows three DLIT images and three EL images of a mc-Si solar cell for applied voltages ranging from -10 to -16 V. Comparing the two sets of images, we find a very good correlation between the reverse-EL and reverse-DLIT signal since the emission of light is always accompanied by a temperature increase. This confirms the results of previous investigations.[11,52]

For those spots marked by white circles in Fig. 6, Fig. 7(a) shows the complete reverse characteristic of the luminescence emission and Fig. 7(b) shows the characteristic of the DLIT signal given in absolute values of reverse current density. In order to allow for a direct comparison of sites with different absolute signal amplitudes, Fig. 7(c) shows luminescence as well as thermography data normalized to the signal measured at -20 V. The very good correspondence of the luminescence emission signal and the reverse
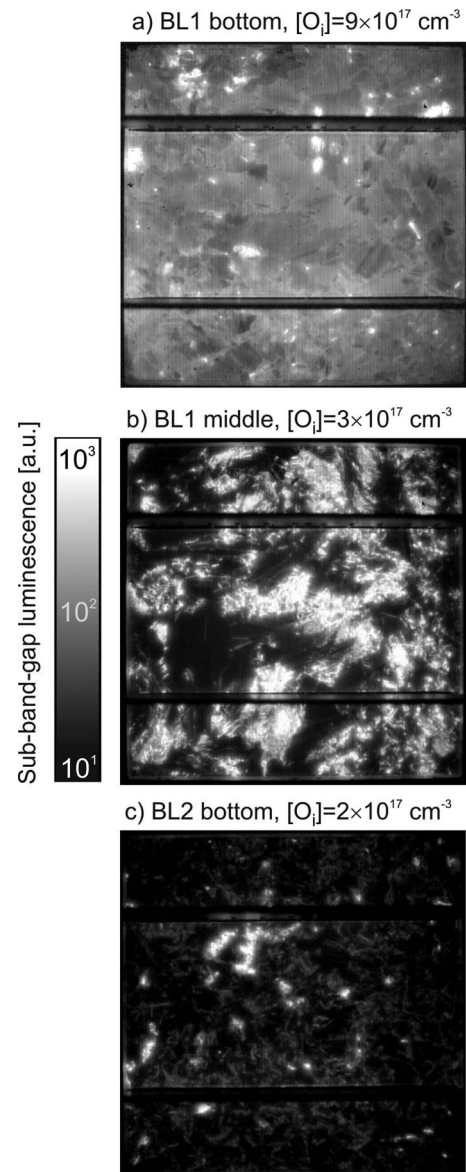

FIG. 5. Integral subband-gap luminescence emission in the wavelength range between 1450 and 1700 nm detected from 0.6 V forward-biased block-cast mc-Si solar cells taken from two blocks (BL). The cells are taken from different positions out of the same block having a high interstitial oxygen concentration ranging from 9×10^{17} cm^3 at the bottom to 1×10^{17} cm^3 at the top. While cell (a) taken from the bottom-near region shows a homogeneous luminescence emission superimposed by some bright spots, cells (b) and (c) taken from the center and top regions, respectively, only show the characteristic local subband-gap luminescence emission.

current density shown in Fig. 7(c) indicates that the luminescence emission at one site depends linearly on the local current flow at that site. As summarized in Table I and as discussed below, we distinguish between three different breakdown types detectable by both methods, reverse-EL and reverse-DLIT. Based on the analysis of reverse-biased EL alone, a similar categorization was proposed previously.[11,55]

As can be seen in Fig. 7, some sites (green curve, data labeled by 1 and I) show a linear to superlinear breakdown characteristic with a well detectable heat and light emission at around -10 V, while others (blue curve, data labeled by 2 and II) show breakdown characteristics starting at reverse
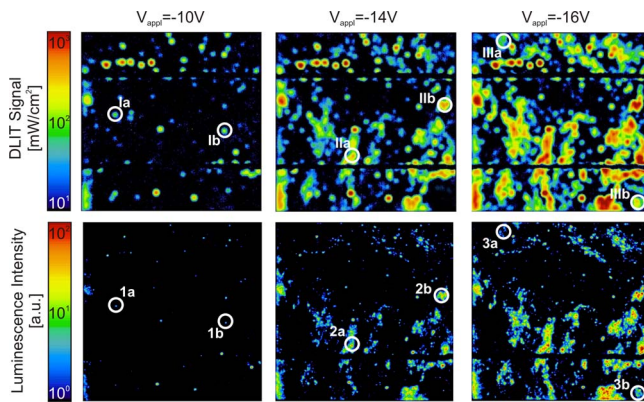
FIG. 6. (Color online) DLIT and EL images of a mc-Si solar cell at reverse-bias voltages ranging from −10 to −16 V. The positions marked with white circles are randomly chosen for detailed investigations of the local reverse characteristics (see Fig. 7).

voltages above −12 V following a soft monoexponential characteristic with an exponential prefactor of 0.72 ± 0.02. The thermal as well as the light emission of the latter sites tend to increase much more rapidly with increasing reverse voltage. Above −16 V, sites (red curve, data labeled by 3 and
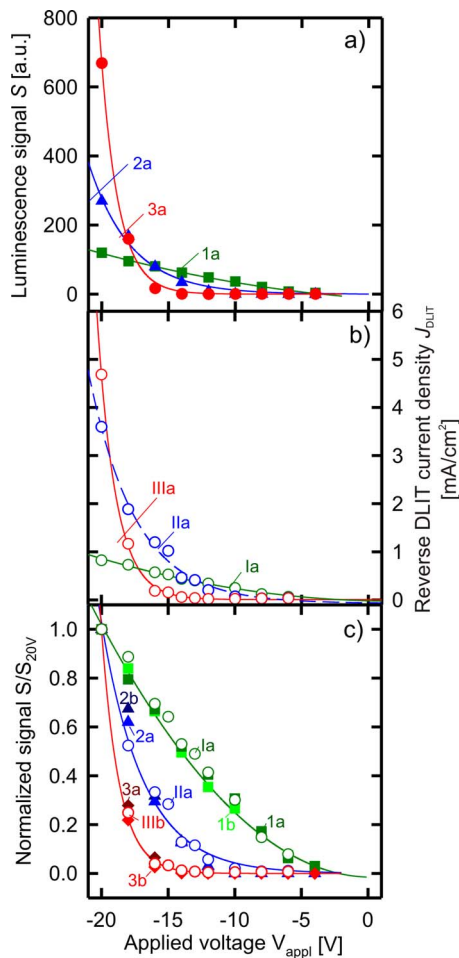

FIG. 7. (Color online) Local reverse characteristics of (a) luminescence emission and (b) DLIT current density for regions indicated by white circles in Fig. 6. Graph (c) shows the data from (a) and (b) normalized to the signal measured at −20 V. The correspondence of the luminescence and DLIT data indicates that the luminescence emission is proportional to the local current density.

III) appear which show an extremely rapid increase in the light and thermal emission with increasing reverse voltage. From the analysis of a larger number of solar cells, we know that the number of sites characterized by a "hard monoexponential" characteristic with an exponential prefactor of 0.31 ± 0.02 is smaller compared to the number of all other prebreakdown sites. As can be seen from the areas marked green in Fig. 2, this latter type of breakdown is only observed in regions of high EL intensity where no defect-related luminescence is detected. This is in good correspondence to Kwapil *et al.*[11] reporting on a negative correlation between breakdown sites showing a "hard-exponential" behavior and areas of increased recombination activity.

As has recently been proposed by Breitenstein *et al.*,[56] images of the local TC of the breakdown allow for a more detailed analysis of the underlying physical mechanism. Therefore, exemplarily, Fig. 8 shows an image of the local TC of the breakdown current calculated from two DLIT images measured at an applied voltage of −16 V and at 293 and 303 K, respectively. The TC indicates the relative current change in percent per kelvin temperature increase. The white circles indicate the same regions, as in Fig. 6. Sites IIIa and IIIb, characterized by a hard-exponential breakdown characteristic, are found to have a clearly negative TC value of about −2. Investigating mc-Si solar cells from several different suppliers, we have always found that those breakdown sites with a hard-exponential reverse characteristic show a negative TC, as expected for AB. These results confirm first investigations by Wagner *et al.*[57] and more detailed investigations by Bauer *et al.*[58]

With decreasing temperature, the charge carriers can gain enough energy for AB since the number of phonons available for scattering decreases. Moreover, AB will only occur in areas of low crystallographic defect and impurity concentrations since only in these regions is the scattering probability low enough for charge carriers to gain enough energy in the electric field. If, additionally, the electric field strength is locally enhanced, breakdown will occur preferentially at those sites. Such an enhancement occurs at etch pits where the junction tends to be thinner, resulting in an increase in the local electric field strength. This effect has first been discussed by Shields[59] and by Senitzky and Moll[60] showing that AB occurs at lower voltages for junctions with smaller radii of curvature. More recently, first experimental results by Kasemann *et al.*[55] and a systematic study by Bauer *et al.*[58] provided clear experimental evidence that the strongly curved *p-n* junction at etch pits exhibits an electrostatic field strong enough to result in a local AB.

For those breakdown sites, showing a soft-exponential or linear to superlinear behavior, it is more difficult to determine the TC. While those sites showing a soft-exponential behavior tend to have a slightly negative TC, sites showing a linear to superlinear behavior tend to have a positive TC. The underlying physical mechanisms explaining the breakdown are not yet understood. Most likely, a multistep field emission process can be held responsible in both cases.[57] Depending on the type, density, and nature of defects in the band gap, either a linear to superlinear or a soft-exponential behavior is found. Crystallographic defects formed during the

TABLE I. Classification of the breakdown characteristics of block-cast mc-Si solar cells.

Breakdown characteristic	Mechanism	TC of breakdown current at room temperature
Linear, superlinear (green data set)	Probably IFE; tunneling assisted process via energy states in the band gap or in the vicinity conducting channels	Ambiguous around zero
Soft exponential (blue data set)	IFE with trap-assisted tunneling or trap-assisted avalanche, strong correlation with defect-rich areas showing a high recombination activity	Slightly negative
Hard exponential (red data set)	AB due to high local electric fields (e.g., at thin emitter sites)	Clearly negative

solidification process of mc-Si are often found to penetrate through several centimeters of the crystal along the direction of solidification. Therefore, especially in regions of high dislocation density, conducting channels extending from the solar cell base region into the *p-n* junction should exist. Our results suggest that defect states in or in the vicinity of these channels support a multistep field emission process.

IV. CONCLUSION

The phenomenon of local junction breakdown in industrial mc-Si solar cells is investigated by camera-based DLIT and EL imaging. The breakdown occurs locally at specific sites and is associated with an increase in temperature at those sites. For the majority of these sites, the breakdown is associated with the emission of whitish light. This light is well detectable using a silicon charge coupled device camera. Moreover, an additional light emission is found in some areas to occur in the subband-gap range at wavelengths between 1400 and 1700 nm. This emission occurs under forward bias and is due to defect-related radiative recombination of charge carriers. Even though there are areas where both effects, reverse-bias luminescence and subband-gap luminescence, are detected, we have not found a clear one-to-one correlation. Thus, we expect that different types of impurities or clusters of impurities, trapped at or in the vicinity of dislocations, can be held responsible for both effects.

Our assumptions are supported by a literature survey addressing local junction breakdown as well as defect-related luminescence emission in silicon. Moreover, we provide clear experimental evidence that oxygen plays a major role in the explanation of the defect-related subband-gap lumines-

cence. This evidence results from EDX studies of precipitates at dislocation sites showing a clear $K\alpha_1$ oxygen peak and the experimental findings that mc-Si solar cells with a high interstitial oxygen concentration for which bulk precipitation of oxygen is expected to show a homogenously distributed subband-gap luminescence signal.

However, more detailed studies on a larger number of cells are required in order to confirm the classification given above. From the finding that breakdown preferentially occurs at decorated crystallographic defects, we deduce the necessity for a careful analysis of mc-Si solar cells made from upgraded metallurgical-grade (UMG) silicon. Even though the efficiency of solar cells made from UMG silicon is basically not affected[61] by the higher impurity content of the feedstock material, these solar cells are known to suffer from considerably lower breakdown voltages. Studies on the microscopic level may result in a better understanding of the nature of the defects causing the local junction breakdown and the subband-gap luminescence, respectively. Once these mechanisms are understood, strategies for their avoidance might be deduced. Since the breakdown voltage limits the number of cells in the string of a solar module, a higher breakdown voltage would directly affect the module design, allowing longer string lengths.
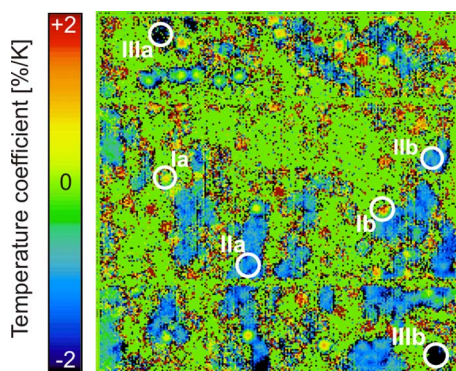
ACKNOWLEDGMENTS

FIG. 8. (Color online) Image of the TC of the breakdown current calculated from two DLIT images measured at an applied voltage of −16 V and at 293 and 303 K, respectively. The TC indicates relative current change in percent per kelvin temperature increase. The white circles indicate the same regions as in Fig. 6.

[1] S. M. Sze and G. Gibbons, Appl. Phys. Lett. **8**, 111 (1966).
[2] A. Woyte, J. Nijs, and R. Belmans, Sol. Energy **74**, 217 (2003).
[3] R. Newman, W. C. Dash, R. N. Hall, and W. E. Burch, Phys. Rev. **98**, 1536 (1955).
[4] A. Goetzberger and W. Shockley, Bull. Am. Phys. Soc. **4**, 409 (1955).
[5] R. Newman, Phys. Rev. **100**, 700 (1955).
[6] A. Simo and S. Martinuzzi, *Proceedings of the 21st Photovoltaic Specialists Conference*, Orlando (IEEE, New York, 1990), p. 800.
[7] J. W. Bishop, Sol. Cells **26**, 335 (1989).
[8] F. Dreckschmidt, T. Kaden, H. Fiedler, and H. J. Möller, *Proceedings of the 22nd European Photovoltaic Solar Energy Conference*, Milano, Italy (WIP, Munich, 2007), p. 238.
[9] K. Bothe, D. Hinken, K. Ramspeck, A. Kitiyanan, and T. Fuyuki, Proceedings of the 17th Photovoltaic Science and Engineering Conference, 2007, p. 261.
[10] M. Kasemann, W. Kwapil, M. C. Schubert, H. Habenicht, B. Walter, M. The, S. Kontermann, S. Rein, O. Breitenstein, J. Bauer, A. Lotnyk, B. Michl, H. Nagel, A. Schütt, J. Carstensen, H. Föll, T. Trupke, Y. Augarten, H. Kampwerth, R. A. Bardos, S. Pingel, J. Berghold, W. Warta, and S. W. Glunz, *Proceedings of the 33rd Photovoltaic Specialists Conference*, San Diego (IEEE, New York, 2008).
[11] W. Kwapil, M. Kasemann, J. Giesecke, B. Michl, and W. Warta, *Proceedings of the 23rd European Photovoltaic Solar Energy Conference*, Valen-

cia, Spain (WIP, Munich, 2008), p. 1797.

[12]T. Fuyuki, H. Kondo, Y. Kaji, Y. Takahashi, T. Yamazaki, and Y. Uraoka, *Proceedings of the 20th European Photovoltaic Solar Energy Conference*, Barcelona, Spain (WIP, Munich, 2005), p. 667.

[13]H. Kressel, RCA Rev. **28**, 175 (1967).

[14]S. Mahadevan, S. M. Hardas, and G. Suryan, Phys. Status Solidi A **8**, 335 (1971).

[15]K. G. McKay and K. B. McAfee, Phys. Rev. **91**, 1079 (1953).

[16]K. G. McKay, Phys. Rev. **94**, 877 (1954).

[17]K. G. McKay and A. G. Chynoweth, Phys. Rev. **99**, 1648 (1955).

[18]A. G. Chynoweth and K. G. McKay, Phys. Rev. **102**, 369 (1956).

[19]A. G. Chynoweth and K. G. McKay, Phys. Rev. **106**, 418 (1957).

[20]The TC can be defined for the breakdown current at a constant voltage as well as for the breakdown voltage at a constant current. While for AB the TC is negative for the first definition, it is positive for the latter one.

[21]A. G. Chynoweth and G. L. Pearson, J. Appl. Phys. **29**, 1103 (1958).

[22]A. R. Plummer, J. Electron. Control **5**, 405 (1958).

[23]M. Kikuchi and K. Tachikawa, J. Phys. Soc. Jpn. **15**, 835 (1960).

[24]M. Kikuchi, J. Phys. Soc. Jpn. **15**, 1822 (1960).

[25]T. Buonassisi, A. A. Istratov, M. D. Pickett, M. Heuer, J. P. Kalejs, G. Hahn, M. A. Marcus, B. Lai, Z. Cai, S. M. Heald, T. F. Ciszek, R. F. Clark, D. W. Cunningham, A. M. Gabor, R. Jonczyk, S. Narayanan, E. Sauar, and E. R. Weber, Prog. Photovoltaics **14**, 513 (2006).

[26]A. Goetzberger and C. Stephens, J. Appl. Phys. **32**, 2646 (1961).

[27]W. Shockley, Solid-State Electron. **2**, 35 (1961).

[28]N. Akil, S. E. Kerns, D. V. Kerns, A. Hoffmann, and J.-P. Charles, Appl. Phys. Lett. **73**, 871 (1998).

[29]N. Akil, S. E. Kerns, D. V. Kerns, A. Hoffmann, and J.-P. Charles, IEEE Trans. Electron Devices **46**, 1022 (1999).

[30]N. A. Drozdov, A. A. Patrin, and V. D. Tkachev, Sov. Phys. JETP **23**, 597 (1976).

[31]C. Cabanel and J. Y. Laval, J. Appl. Phys. **67**, 1425 (1990).

[32]M. Kittler, W. Seifert, and V. Higgs, Phys. Status Solidi A **137**, 327 (1993).

[33]T. S. Fell, P. R. Wilshaw, and M. D. D. Coteau, Phys. Status Solidi A **138**, 695 (1993).

[34]S. A. McHugo, A. C. Thompson, I. Périchaud, and S. Martinuzzi, Appl. Phys. Lett. **72**, 3482 (1998).

[35]Y. Koshka, S. Ostapenko, I. Tarasov, S. McHugo, and J. P. Kaleys, Appl. Phys. Lett. **74**, 1555 (1999).

[36]I. Tarasov, S. Ostapenko, V. Feifer, S. McHugo, S. V. Koveshnikov, J. Weber, C. Haessler, and E.-U. Reisner, Physica B **273–274**, 549 (1999).

[37]S. Ostapenko, I. Tarasov, J. P. Kalejs, C. Haessler, and E.-U. Reisner, Semicond. Sci. Technol. **15**, 840 (2000).

[38]M. Tajima, M. Tokita, and M. Warashina, Mater. Sci. Forum **196–201**, 1749 (1995).

[39]M. Tajima, J. Cryst. Growth **103**, 1 (1990).

[40]N. S. Minaev and A. V. Mudryi, Phys. Status Solidi A **68**, 561 (1981).

[41]O. King and D. G. Hall, Phys. Rev. B **50**, 10661 (1994).

[42]Y. Kitagawara, R. Hoshi, and T. Takenaka, J. Electrochem. Soc. **139**, 2277 (1992).

[43]H. Sugimoto, K. Araki, M. Tajima, T. Eguchi, I. Yamaga, M. Dhamrin, K. Kamisako, and T. Saitoh, J. Appl. Phys. **102**, 054506 (2007).

[44]O. Breitenstein, J. P. Rakotoniaina, and M. H. Al Rifai, Prog. Photovoltaics **11**, 515 (2003).

[45]Y. Takahashi, Y. Kaji, A. Ogane, Y. Uraoka, and T. Fuyuki, *Proceedings of the Fourth World Conference on Photovoltaic Energy Conversion*, Waikoloa, HI (IEEE, New York, 2006), p. 924.

[46]O. Breitenstein and M. Langenkamp, *Lock-in Thermography*, Springer Series in Advanced Microelectronics (Springer, Berlin, 2003), Vol. 10.

[47]S. D. Feldman, F. H. Seymour, T. R. Ohno, V. Kaydanov, and R. T. Collins, Mater. Res. Soc. Symp. Proc. **763**, B5.10.1 (2003).

[48]K. Bothe, P. Pohl, J. Schmidt, T. Weber, P. Altermatt, B. Fischer, and R. Brendel, *Proceedings of the 21st European Photovoltaic Solar Energy Conference*, Dresden, Germany (WIP, Munich, 2006), p. 597.

[49]R. Nitecki and B. Pohoryles, Appl. Phys. A: Mater. Sci. Process. **36**, 55 (1985).

[50]Q. Li and R. W. Dutton, IEEE Trans. Electron Devices **38**, 936 (1991).

[51]H. J. Möller, C. Funke, A. Lawerenz, S. Riedel, and M. Werner, Sol. Energy Mater. Sol. Cells **72**, 403 (2002).

[52]O. Breitenstein, J. Bauer, J.-M. Wagner, H. Blumtritt, A. Lotnyk, M. Kasemann, W. Kwapil, and W. Warta, *Proceedings of the 34th Photovoltaic Specialists Conference*, Philadelphia (IEEE, New York, in press).

[53]M. Wagner and T. Weber, *Proceedings of the 23rd European Photovoltaic Solar Energy Conference*, Valencia, Spain (WIP, Munich, 2008), p. 1338.

[54]O. Breitenstein, J. Bauer, T. Trupke, and R. A. Bardos, Prog. Photovoltaics **16**, 325 (2008).

[55]M. Kasemann, W. Kwapil, B. Walter, J. Giesecke, B. Michl, M. The, J.-M. Wagner, J. Bauer, A. Schütt, J. Carstensen, S. Kluska, F. Granek, H. Kampwerth, P. Gundel, M. C. Schubert, R. A. Bardos, H. Föll, H. Nagel, P. Würfel, T. Trupke, O. Breitenstein, M. Hermle, W. Warta, and S. W. Glunz, *Proceedings of the 23rd European Photovoltaic Solar Energy Conference*, Valencia, Spain (WIP, Munich, 2008), p. 965.

[56]O. Breitenstein, J. Bauer, J.-M. Wagner, and A. Lotnyk, Prog. Photovoltaics **16**, 679 (2008).

[57]J.-M. Wagner, J. Bauer, A. Lotnyk, and O. Breitenstein, *Proceedings of the 23rd European Photovoltaic Solar Energy Conference*, Valencia, Spain (WIP, Munich, 2008), p. 1164.

[58]J. Bauer, J.-M. Wagner, A. Lotnyk, H. Blumtritt, B. Lim, J. Schmidt, and O. Breitenstein, Phys. Status Solidi (RRL) **3**, 40 (2009).

[59]J. Shields, J. Electron. Control **4**, 58 (1958).

[60]B. Senitzky and J. L. Moll, Phys. Rev. **110**, 612 (1958).

[61]V. Hoffmann, K. Petter, J. Djordjevic-Reiss, E. Enebakk, J. T. Håkedal, R. Tronstad, T. Vlasenko, I. Buchovskaja, S. Beringov, and M. Bauer, *Proceedings of the 23rd European Photovoltaic Solar Energy Conference*, Valencia, Spain (WIP, Munich, 2008), p. 1117.